Layer-resolved magnetic exchange interactions of surfaces of late 3*d* elements: Effects of electronic correlations

S. Keshavarz,[1] Y. O. Kvashnin,[1] I. Di Marco,[1] A. Delin,[1,2] M. I. Katsnelson,[3,4] A. I. Lichtenstein,[4,5] and O. Eriksson[1]

[1]*Uppsala University, Department of Physics and Astronomy, Division of Materials Theory, Box 516, SE-751 20 Uppsala, Sweden*
[2]*KTH Royal Institute of Technology, Department of Materials and Nano Physics, Electrum 229, SE-164 40 Kista, Sweden*
[3]*Radboud University of Nijmegen, Institute for Molecules and Materials, Heijendaalseweg 135, 6525 AJ Nijmegen, The Netherlands*
[4]*Theoretical Physics and Applied Mathematics Department, Ural Federal University, Mira Street 19, 620002 Ekaterinburg, Russia*
[5]*Institute of Theoretical Physics, University of Hamburg, Jungiusstrasse 9, 20355 Hamburg, Germany*
(Received 23 June 2015; published 28 October 2015)

We present the results of an *ab initio* study of the magnetic properties of Fe, Co, and Ni surfaces. In particular, we discuss their electronic structure and magnetic exchange interactions (J_{ij}), as obtained by means of a combination of density functional theory and dynamical mean-field theory. All studied systems have a pronounced tendency to ferromagnetism both for bulk and surface atoms. The presence of narrowband surface states is shown to enhance the magnetic moment as well as the exchange couplings. The most interesting results were obtained for the Fe surface where the atoms have a tendency to couple antiferromagnetically with each other. This interaction is relatively small when compared to interlayer ferromagnetic interaction, and it depends strongly on the lattice parameter. Local correlation effects are shown to lead to strong changes of the overall shape of the spectral functions. However, they seem not to play a decisive role in the overall picture of magnetic couplings studied here. We have also investigated the influence of correlations on the spin and orbital moments of bulklike and surface atoms. We found that dynamical correlations in general lead to enhanced values of the orbital moment.

I. INTRODUCTION

Bulk Fe, Co, and Ni are all classical examples of ferromagnets. However, when confined to two dimensions, these transition metals (TM) show a large panorama of fascinating magnetic properties and phenomena [1–3]. For instance, thin layers of these atoms may show antiferromagnetic (AFM) behavior or even noncollinear spin structures, depending on the film thickness and/or the substrate [4–6]. The latter is known to play an important role, producing strains due to lattice mismatch and hybridizing with the TM states [7–10]. All the above-mentioned effects contribute to the magnetic exchange interactions (J_{ij}), which are the relevant parameters of an effective spin-Hamiltonian that determine the Curie temperature and magnon dispersion of the material. The latter two quantities are of particular importance for technological applications in, e.g., spintronic memory and logic devices. Hence, a fundamental understanding of the magnetic properties of these systems is needed.

The magnetism of surfaces has been of interest for quite some time. Initial studies were mainly focused on differences between surfaces and bulk properties. For instance, experimentally it was discussed for some time that fcc Ni layers on top of a Cu substrate produced magnetically "dead" layers, with an absence of magnetic moments [11]. However, subsequent experiments [12] and theory [13–15] suggested that the spin moments at surfaces in general are enhanced, since the bands are narrower. Later on, relativistic electronic structure theory could analyze also the orbital moments of surfaces, and here the enhancement of the surface magnetism was found to be even larger than the spin contribution for bcc Fe, hcp Co, and fcc Ni [16–18]. These theoretical predictions were confirmed by experiments using x-ray magnetic circular dichroism [19].

Computational modeling is very important to investigate magnetic properties, as it gives a material-specific description and makes it possible to disentangle all the relevant contributions. Density functional theory (DFT) and its formal extensions [20–22] give an excellent parameter-free description of ground-state properties of magnetic metals, including bulk structures as well as systems without three-dimensional periodicity such as surfaces, interfaces, thin films, disordered alloys, and nanoparticles. However, several studies have emphasized the importance of including strong correlation effects in the electronic structure of bulk Fe, Co, and Ni. For instance, noncoherent features such as Hubbard bands and satellites, which appear in the excitation spectra of the photoemission experiments [23,24], cannot be described by the local density approximation (LDA) and/or the generalized gradient approximation (GGA). In addition, LDA calculations predict a too wide majority spin 3*d* band and overestimate the spin splitting for these materials [25–28].

Correlation effects in transition metals are expected to be even more pronounced for the surface atoms due to narrower bands and reduced coordination numbers. In this article, we report on a computational study of surface magnetism of TM slabs. The main focus is on the calculations of magnetic moments and interatomic exchange interactions (J_{ij}). The simulations are based on a combination of DFT and dynamical mean-field theory (DMFT). This technique, which is usually referred to as LDA+DMFT, is the current state-of-the-art method to study strong correlations in materials at finite temperature [29–31].

To the best of our knowledge, LDA+DMFT has not been previously applied to the exchange interactions of transition-metals surfaces. Even for standard DFT, such simulations are rare, as most attention was focused on thin films on various substrates [10,32–35]. One of the reasons for this is that much software is still based on the atomic-sphere approximation (ASA), which limits their use for studying

surfaces, or low-dimensional systems in general. The methods used in the present work do not have this limitation.

This paper is organized as follows. In Sec. II we briefly explain the computational scheme used in this work, as well as the implementation of the formalism described in Ref. [36] for evaluating the exchange parameters. The result of our electronic structure calculations and exchange interactions for Fe, Co, and Ni surfaces are presented in Sec. III. The following section reports our investigation of the orbital polarizations for each slab. Finally, we draw our conclusions, which will be followed by three Appendixes. Appendix A concerns the influence of the Hubbard U value, Appendix B is about the effect of full self-consistency over the charge density on the exchange parameters, and Appendix C describes renormalization factors due to many-body effects.

II. THEORY

The electronic structure as well as the magnetic properties of the TM slabs were investigated in the framework of the scalar-relativistic full-potential linear muffin-tin orbital (FP-LMTO) code RSPt [37]. Due to the full-potential character, the code does not have limitations dictated by the geometry of the problem under consideration. Moreover, due to the small number of basis functions, RSPt is particularly suitable for LDA+DMFT simulations with full self-consistency over self-energy and electron density. The details of this implementation were presented elsewhere [27,37–39] and will not be repeated here. We redirect the reader to those references for a detailed overview of our formalism.

Once the electronic structure was converged, the magnetic excitations were mapped onto the Heisenberg Hamiltonian:

$$\hat{H} = -\sum_{i \neq j} J_{ij} \vec{e}_i \vec{e}_j, \qquad (1)$$

where J_{ij} is an exchange interaction between the spins, located at sites i and j, and $\vec{e}_i$ is a unity vector along the magnetization direction at the corresponding site. We extracted the pairwise exchange interactions by employing the method of infinitesimal rotation of the spins. The exchange parameters were computed using the local magnetic force approach [36,40], which reads

$$J_{ij} = \frac{1}{4}\text{Tr}_{\omega,L}\big[\hat{\Sigma}_i^s(i\omega_n)G_{ij}^\uparrow(i\omega_n)\hat{\Sigma}_j^s(i\omega_n)G_{ji}^\downarrow(i\omega_n)\big], \qquad (2)$$

where G_{ij}^σ is the intersite Green's function, σ denotes spin projection ($\sigma = \{\uparrow, \downarrow\}$), and the trace is taken over the fermionic Matsubara frequencies $i\omega_n$ and the states characterized by an angular momentum quantum number L. The crucial quantity in Eq. (2) is the dynamical on-site exchange potential:

$$\hat{\Sigma}_i^s(i\omega_n) \equiv (\hat{H}_i^\uparrow - \hat{H}_i^\downarrow) + (\hat{\Sigma}_i^\uparrow(i\omega_n) - \hat{\Sigma}_i^\downarrow(i\omega_n)), \qquad (3)$$

where $\hat{H}_i^\sigma$ is the local Hamiltonian matrix obtained by solving the DFT equations, and Σ_i^σ is the self-energy describing the electronic correlations. The self-energy appears only for LDA+DMFT calculations, and also enters the expression of the Green's function as

$$\hat{G}_{ij}(i\omega_n) = \langle i | \frac{1}{i\omega_n - \hat{H} - \hat{\Sigma}(i\omega_n)} | j \rangle. \qquad (4)$$

More details about the evaluation of the exchange interactions, particularly in relation to the basis set used for the local orbitals, can be found in Ref. [41].

For the sake of simplicity, relativistic effects will not be considered in our work unless explicitly stated. These effects give rise to other types of magnetic interactions, such as anisotropic exchange couplings and magnetocrystalline anisotropy. However, the bilinear term considered in the present work is usually the leading one. For instance, it was recently shown for Fe/Rh(001) that by considering Heisenberg interactions only, it is possible to obtain a very detailed picture of magnetic excitations, yielding excellent agreement with experiment [34]. Nevertheless, we performed a few additional simulations with spin-orbit coupling included in order to analyze the enhancement of the orbital magnetism at the surfaces, which is a very important problem in materials science. These results will be presented at the end of the paper.

A. Computational details

DFT simulations were performed by using the LDA as an exchange-correlation functional. After the convergence, we applied the LDA+DMFT technique for a selected set of TM $3d$ orbitals. The k integration over the irreducible wedge of the Brillouin zone has been performed using $24 \times 24 \times 24$ points for bulk and $24 \times 24 \times 1$ points for the slabs. We have performed relaxation of the topmost layers of the Fe slab, which are known to be quite small in these systems [42]. In the LDA for Fe we obtained a $0.1\%\,(1\%)$ reduction of the surface (subsurface) magnetic moments with respect to unrelaxed slabs (truncated bulk). For Co and Ni, we did not perform extensive tests, as we expect the changes induced by the relaxation to be even smaller. In fact, these changes are proportional to the difference between bulk and surface spin moments, which is much larger for Fe than for Co and Ni. Therefore, to avoid presenting two sets of similar results and to facilitate comparison with similar studies, our analysis will be limited to unrelaxed slabs, where the interatomic distances depend solely on the bulk lattice parameter. The latter was chosen as obtained from experiments, i.e., 2.86 Å for bcc Fe, 3.52 Å for fcc Ni, and 2.51 Å for hcp Co [43]. For the latter, the distance between the hexagonal planes was chosen as 4.07 Å [43]. The free-standing slabs of Fe, Co, and Ni have been modeled using 15 layers of their bulk structure repeated in the (001) direction for Fe and Ni, while the (0001) direction was used in the case of Co. Since three-dimensional periodic boundary conditions are used, a 27-Å-thick layer of vacuum was used to construct a supercell.

LDA+DMFT simulations were performed for a temperature of 400 K. The effective impurity problem arising in DMFT was solved through the spin-polarized T-matrix fluctuation-exchange (SPTF) solver [44]. Since the latter is a perturbative approach, it can only be applied to systems with moderate correlations and in the metallic regime of the Mott-Hubbard transition. SPTF is usually applied by using the static part of the self-energy as a double-counting correction term. This choice has been used for all DMFT simulations throughout the paper.

For $3d$ orbitals, where the electrons are supposed to show more atomiclike features, the Coulomb interaction can be

parametrized via Slater integrals F^n [45]:

$$U = F^0, \quad J = \frac{F^2 + F^4}{14}, \tag{5}$$

where U is the Hubbard parameter and J is Hund's exchange. The values of U and J can be either extracted from experiments or calculated from first-principles. In this work, we have taken their values from the literature [25,26,44]. LDA+DMFT calculations for Fe and Co were done utilizing $U = 2.3$ eV and $J = 0.9$ eV, while for Ni, $U = 3$ eV and $J = 0.9$ eV were chosen. To see the effect of U on the spectra and exchange parameters, we have performed some test calculations using larger values of U for surface and subsurface atoms while keeping the previous value unchanged for the inner layers. Although it is known that the choice of U affects the intensity and the position of satellites in the valence-band spectra, e.g., as reported in Ref. [27], our results suggest that the exchange parameters are marginally affected by varying the U value. This analysis is illustrated in Appendix A.

Finally, we performed extensive tests to analyze the role of self-consistency over the electron density in the LDA+DMFT cycle. We focused on spectral functions and exchange interactions for a seven-layer slab. These results are presented in Appendix B. Our general conclusion is that updating the electron density in the LDA+DMFT cycle introduces minor corrections for the transition-metals surfaces, at least concerning the magnetic properties. In light of these minor changes, as well as for computational efficiency, we performed simulations of 15-layer slabs by keeping the electron density unchanged.

III. RESULTS

We consider free-standing slabs of $3d$ transition metals in their most stable magnetic structure below the Curie temperature. The exchange interaction is calculated for different layers as a function of the interatomic distance between pair of atoms. These calculations are aimed at understanding in detail the differences between bulk and surface, and also at seeing how the local dynamical correlations affect the exchange interactions. In the next few sections, we will elaborate on these issues separately for each element.

A. Fe

1. The (001) surface

It is important to address first the convergence of the relevant magnetic properties with respect to the thickness of the slab. We present this analysis only for Fe for brevity. In Fig. 1, layer-resolved Fe-$3d$ projected spin moments are reported for slabs of different thickness. These calculations reveal long-range damped oscillations of the local moments when going from the outermost layer to the innermost one. This behavior is due to the surface-induced changes in the magnetism of the itinerant ferromagnets (Friedel oscillations) [46,47]. In principle, the formation of the quantum states in the finite-size slabs is accompanied by the creation of a barrier on the surface that leads to a different electronic structure around the Fermi level (E_F). In the cases of Fe, Co, and Ni, the magnetic moment of the innermost layer reached the bulk value, with
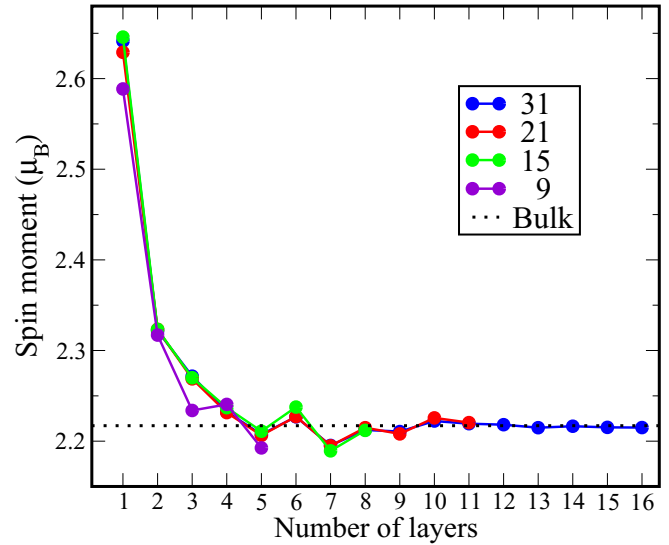
FIG. 1. (Color online) Layer-resolved Fe-$3d$ projected spin moment for different slabs, whose thickness varies from 9 to 31 layers. The layers are numbered from 1 (surface) to N_{max} (the innermost layer). N_{max} is equal to the total number of layers in the slab plus 1, divided by 2.

a difference smaller than 1%, for slabs of 15 layers. For this size, the exchange interactions of the innermost layer of Co and Ni slabs were equal to those of their bulk up to 0.5%. For Fe, however, a slightly larger difference was obtained, of about 1.2%, which was due to the difficulties in matching the same special points for the sampling of two-dimensional and three-dimensional Brillouin zones. Finally, an analogous convergence of the electronic structure can be observed in Fig. 2, where the projected density of states (PDOS) of the innermost layer is compared with the PDOS of the bulk for the 15-layer slab. The curves do not exhibit any visible difference on the scale of interest, for both LDA and LDA+DMFT.

Next we have analyzed the differences in the PDOS of the surface atoms and that of the innermost layer. These results obtained in LDA and LDA+DMFT are shown in Fig. 3. The PDOS at the surface is very different from the bulk, due to a reduced coordination number, which results in narrower bands and more pronounced correlation effects. Our results are in good agreement with prior studies reported by Grechnev *et al.* [27] and Chuang *et al.* [33]. Note that in the latter
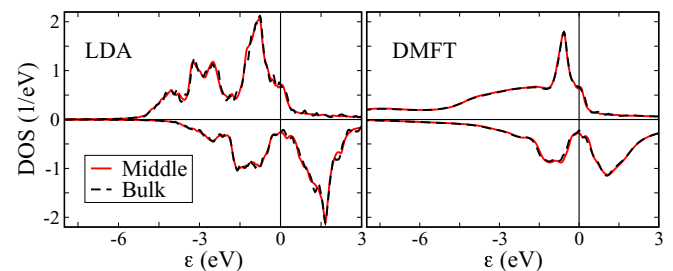
FIG. 2. (Color online) Layer-resolved projected density of states of $3d$ orbitals of the innermost layer (middle) of the Fe slab and of the bulk for majority- and minority-spin components in LDA (left panel) and LDA+DMFT (right panel).
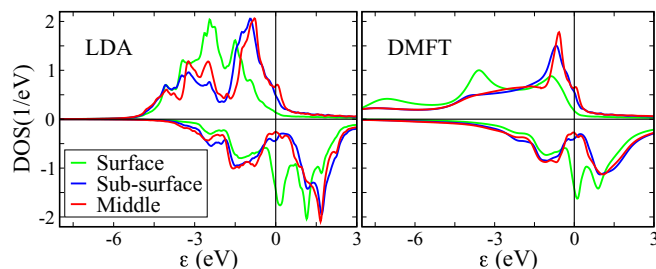
FIG. 3. (Color online) Layer-resolved projected density of states of $3d$ orbitals of a Fe slab for the atoms at the surface, subsurface, and the innermost layer for majority- and minority-spin components in the LDA (left panel) and in the DMFT approach (right panel).

work, the calculations were performed using the generalized gradient approximation, which accounts for some differences with respect to the results reported here.

Figure 3 shows that there are a large number of majority-spin states in the vicinity of E_F for the innermost layer of the Fe slab for both LDA and LDA+DMFT. These states arise mainly due to d_{yz}, d_{xz}, d_{xy} orbitals (not shown here), and they are shifted to lower energies for the atoms sitting at the surface. This results in an effective suppression of spectral weight at E_F. For minority spin, instead, the bulk (innermost layer) PDOS shows just a few states of the t_{2g} character around E_F, where a pseudogap forms. At the surface, the increase of the exchange splitting causes these states to move just across E_F, which results in a drastic increase of the spectral weight. As a result, the spectral weight at the Fermi level arises mainly from one spin channel, which makes the surface behave as a *strong ferromagnet*. The inner layers have instead the characteristics of a *weak ferromagnet*, similarly to the bulk. From Fig. 3, we also notice that the PDOS for the atoms sitting on the subsurface layer does not show substantial differences with respect to the PDOS of the bulk.

We can now focus on a comparison between LDA and LDA+DMFT. Although the overall PDOSs obtained by means of these two methods are quite different, they exhibit very similar behavior in the vicinity of E_F. Given that this region is of primary importance for the exchange interaction, we expect

to obtain similar results within these two approaches, at least as concerns the asymptotic behavior.

From this point on, we focus exclusively on the 15-layer slab. In Fig. 4, the layer-resolved exchange parameters (J_{ij}) are reported for both LDA and LDA+DMFT. For clarity, we report only results for the most physically interesting layers, e.g., the surface, the subsurface, and the innermost layer. Nevertheless, we will make general considerations regarding all layers in the following discussion. The *intralayer* exchange interaction is referred to the case when the two atoms interacting with each other are located in the same layer. The *interlayer* interaction is referred to the case when the two atoms belong to different layers. The layers in the plots are denoted by 1 for the surface, 2 for the subsurface, and so on, analogously to Fig. 1.

The first general consideration to draw from our calculations is that interlayer exchange parameters for atoms in the inner layers are substantially smaller than those for atoms in layers closer to the surface. This trend is observed both for the LDA and in LDA+DMFT. For instance, Fig. 4 shows that the exchange interaction between an atom at the surface and its first nearest neighbor (NN) sitting in the subsurface (blue lines in the right panel) is strongly ferromagnetic. The strength of this exchange interaction is about twice as large as that of an atom in the innermost layer and its first NN in an adjacent layer (pink lines in the left panel of Fig. 4).

A quantitative explanation for the layer dependence of the exchange interactions can be provided by two important factors. First, there is a direct influence of the on-site exchange field at atoms i and j on the corresponding J_{ij} parameter [see Eq. (2)]. Second, the coordination numbers would affect the Hamiltonian $\hat{H}$, the self-energy, and, therefore, the intersite Green's function [see Eq. (3)].

An inspection of Fig. 3 has already revealed that majority- and minority-spin states are more split for the surface atoms. Hence, the local exchange field (Σ^s) is overall larger than its bulk counterpart, which can explain the enhancement of the exchange integrals between surface and subsurface atoms with respect to couplings between more internal (adjacent) layers. Moreover, the surface PDOS is characterized by a larger spin polarization of the Fermi surface in comparison to inner layers. This provides a large number of available states with a certain spin projection right above E_F. Hence, similarly to the double
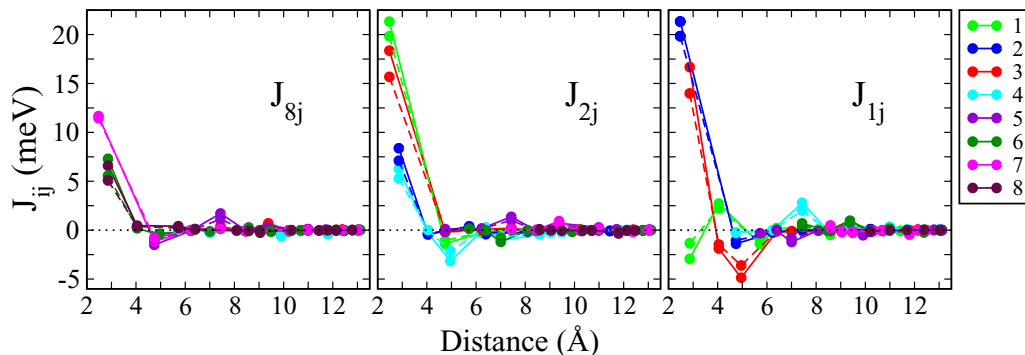
FIG. 4. (Color online) Layer-resolved exchange parameters (J_{ij}) for a 15-layer bcc Fe(001) slab for the case when atom i is located in the innermost layer (left panel), in the subsurface (middle panel), and at the surface (right panel). The solid lines indicate LDA results while the dashed lines represent the LDA+DMFT results. The layer numbering in the legend starts from the surface denoted by 1, the subsurface denoted by 2, and so on. The innermost layer is denoted by 8. The interaction between the surface and layer 9 and others is small and is not shown in these plots.

TABLE I. Orbital-decomposed exchange interaction parameter between two closest neighbors at the surface for the bond vector (010). The reported values are in meV.

	d_{z^2}	$d_{x^2-y^2}$	d_{yz}	d_{xz}	d_{xy}
d_{z^2}	0.81	−1.02	0.36	0.00	0.00
$d_{x^2-y^2}$	−1.02	1.26	−6.26	0.00	0.00
d_{yz}	0.36	−6.26	3.99	0.00	0.00
d_{xz}	0.00	0.00	0.00	−1.07	0.05
d_{xy}	0.00	0.00	0.00	0.05	6.32

FIG. 5. (Color online) (a) and (b) The calculated band structure of a Fe slab for majority- and minority-spin states, respectively, shown with the amount of $3d$ orbital character of the surface atoms (red). (c) The Fermi surface cross section of the minority-spin bands, having the largest contributions from surface $3d$ states. The suggested nesting vector is indicated with the black arrow (the spectra are calculated in the complex energy $E + i\delta$ with $\delta = 0.005$ Ry).

exchange mechanism, electron hopping will be facilitated if it does not have to flip its spin, i.e., if the neighboring moments are parallel to each other. This scenario thus also supports an enhancement of the ferromagnetic interaction with the surface atoms, as obtained in our calculations.

We proceed now to an analysis of the intralayer coupling. An interesting finding of the present investigation is that two Fe atoms at the surface possess an AFM coupling (green lines in the right panel of Fig. 4). Note that this neighborhood corresponds to second NN atoms in bcc structure, and it is therefore always smaller than the leading FM contribution between first NNs. The presence of AFM exchange interactions at the surface is rather surprising, although we note that previous first-principles theory also suggests such a coupling [32]. Fe is known to have a tendency toward AFM coupling for hcp or fcc crystal structures [5,7,10,48] as well as for thin monolayers on some substrates, but seldom in bcc-like environments [33–35]. For example, the exchange coupling between the two neighboring atoms at the surface of Fe clusters was reported to be FM [49].

Here we focus on understanding the origin of this tendency to AFM coupling at the surface. For this purpose we analyze individual orbital contributions to the exchange parameter. The local Hamiltonian for each Fe atom is diagonal in the basis of cubic harmonics, and so is Σ^s from Eq. (2). Having Σ^s in a diagonal form allows us to write each exchange coupling as $J_{12} = \sum_{m_1,m_2} J_{12}^{m_1,m_2}$, where orbital m_1 is located at site 1 and orbital m_2 is at site 2. Exchange interaction between the two closest surface spins in the form of a matrix in orbitals space is shown in Table I. The table hence shows the strength of the exchange interactions of symmetry-resolved states of one atom with symmetry-resolved states of a nearest-neighbor surface atom. The total interaction between these two atoms is obtained by summing all components of Table I. The analysis reveals that there are basically two competing contributions to the J_{ij} between the NN surface moments. A first FM contribution originates from $d_{xy} - d_{xy}$ bonds and $d_{yz} - d_{yz}$ bonds, depending on the bond vector. A second AFM contribution, instead, arises from $d_{yz} - d_{x^2-y^2}$ bonds. This contribution is much stronger in our case, and it overcomes the FM part of the exchange. Similar competition was shown to take place for the next NN exchange couplings in bulk Fe, which corresponds to the same coordination shell that we investigate here [41]. However, the balance between the two contributions can be easily changed by small changes in the NN distance. For example, Chuang et al. [33] reported a FM coupling between the adjacent surface atoms in free-standing

Fe films when using the Ir lattice constant. We have repeated their calculations and obtained the same results. We conclude that the tendency to AFM coupling is innate in the magnetic properties of the Fe surface. This suggests that the primary role of the substrate consists in modifying interatomic distances and not in affecting the electronic structure via direct hybridization, at least for the aforementioned cases.

To obtain a clearer explanation of the AFM interactions at the Fe surface, we have studied its underlying electronic structure in more detail. In Figs. 5(a) and 5(b), we show the spin-polarized band structure projected onto $3d$ states of the surface atoms. The largest contribution of these orbitals to each band is shown with red . As one can see from Fig. 5, the surface states contribute only to the majority-spin bands well below E_F. In contrast, there is a significant weight of them at E_F for the minority-spin channel, particularly near the Γ and X points, which will contribute to the magnetic susceptibility. To strengthen this point, in Fig. 5(c) we show parts of the Fermi surface cross section originating from the bands with a large surface component. One can see that the Fermi surface is nested between the Γ and X points, and the nesting vector is indicated with an arrow in Fig. 5(c). The nesting vector (indicated with the black arrow) is directed along the (100) direction and has a length very close to π/a. This defines a preferable direction for symmetry-breaking in the system, and we suggest that it is connected to the AFM coupling between the NN spins at the surface. We note as well that bulk bcc Fe has similar features of the Fermi surface (see, e.g., Fig. 3 in Ref. [50]). However, the nesting vector connecting the pockets located at the Γ and H points has a much smaller length, which does not lead to the pronounced AFM interaction.

Other considerations can be drawn from the calculated exchange parameters from Fig. 4. AFM intralayer coupling between the closest neighboring atoms at the surface (light-green lines in the right panel) might in principle lead to noncollinear spin configurations. However, we estimate the resulting frustration to be weak, since their interlayer couplings with atoms in the substrate are much larger (dark-blue lines in the right panel).

At the surface, the AFM exchange coupling between the closest neighbors as well as the lower coordination number result in smaller values for the total exchange interactions $J_1 = \sum_j J_{1j}$. This consequence is in qualitative agreement with the LMTO-ASA results reported by Turek *et al.* [32]. A quantitative comparison is, however, not possible for Fe, for which the long-range oscillatory (RKKY-like) behavior of exchange constants makes the value of J_1 strongly dependent on the number of shells taken into account.

Overall, both LDA and LDA+DMFT deliver very consistent results for the exchange parameters, although the latter are slightly smaller. Once the dynamical correlations are introduced, as long as the topology of the Fermi surface is unchanged, the main effect is to produce carrier mass renormalization. A qualitative explanation for the overall decrease of the J_{ij}'s in LDA+DMFT can be found in Ref. [51], where a direct link between the total exchange coupling J_i and the renormalization factor Z is established. However, in a multiorbital case, different (by symmetry) orbitals are characterized by different renormalization factors Z, and therefore there is no simple scaling relation between the overall exchange couplings extracted from LDA and LDA+DMFT. In Appendix C, we show the computed Z-factors for each $3d$ orbital centered on the atom sitting either in the surface, the subsurface, or in the middle layer. One can see that in the case of the Fe slab, the Z-factors for the majority and minority states are very different, reaching the maximal difference for surface electrons (0.53 and 0.73, respectively). More detailed information about the mass enhancement as a measure of the strength of the many-body effects in all of the studied surfaces can be found in Appendix C.

2. The 110 and 111 surfaces

To see whether the AFM exchange coupling between the two nearest neighbors at the surface of Fe can be found in different surface directions, we have performed additional calculations for the surfaces with normal along (110) and (111) directions of bcc Fe. The obtained exchange parameters between the atom at the surface and the ones in any layer (J_{1j}) are shown in Fig. 6. As is clear from the left panel of Fig. 6, the strong FM coupling happens for the NN atoms at the surface of the (110) direction as well as between the second and third NNs. In contrast, such a strong coupling is not observed between the nearest atoms at (111) surface. The reason is that in this case, the closest atoms at the surface are the fourth NN of each other, too far to show significant coupling. As a conclusion, our calculations show that the AFM coupling can only be seen at the surface of the (001) direction.

B. Co

Next, we have considered a slab of hcp Co containing 15 layers repeated in the (0001) direction. In Fig. 7, the PDOSs for the innermost layer, the subsurface, and the surface atoms are shown. The results obtained through both LDA and LDA+DMFT are reported. One can see that the PDOSs for atoms in the innermost layer and in the subsurface are similar around the Fermi level, although their overall shapes are slightly different. For instance, the first peak below E_F for majority-spin states has lower intensity and is located at lower
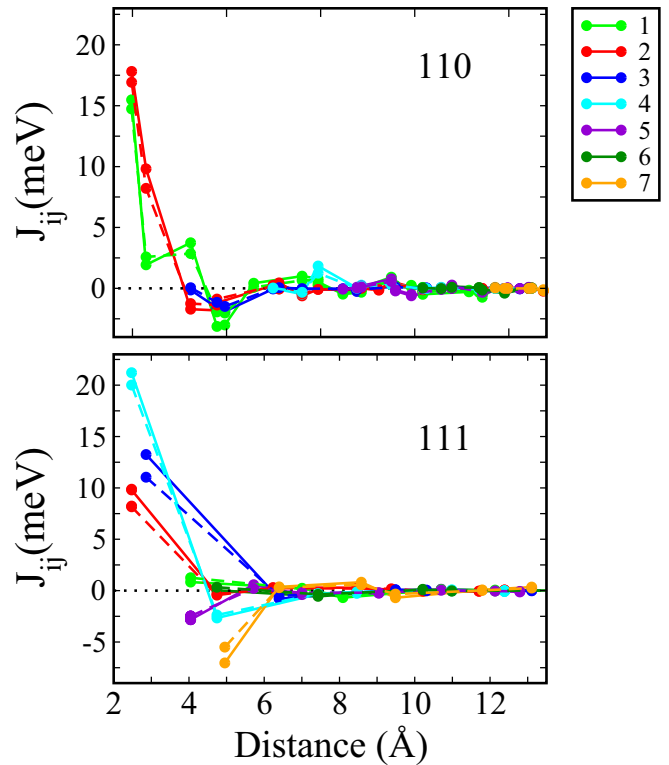
FIG. 6. (Color online) Layer-resolved exchange parameters for a bcc Fe slab in (110) and (111) directions (top and bottom panels, respectively). Here, we only show the results for the case when atom i is located at the surface (J_{1j}). The solid lines indicate LDA results while the dashed lines represent LDA+DMFT results. The layer numbering in the legend starts from the surface denoted by 1, the subsurface denoted by 2, and so on. The results were obtained for a seven-layer slab.

energies for atoms at the subsurface, in comparison with atoms in the innermost layer.

Similar conclusions can be drawn for the surface. The majority-spin PDOS for atoms at the surface shows quite similar features around E_F to that for atoms in the innermost layer. This means that the strong ferromagnetic behavior is found both for the surface of Co as well as the bulk. Nevertheless, the sharp peak below the Fermi level, which
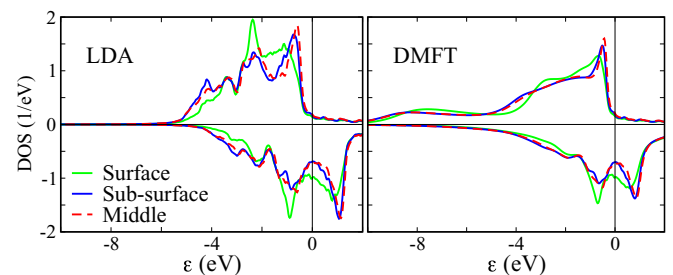
FIG. 7. (Color online) Layer-resolved projected density of states of $3d$ orbitals of a Co slab for the atoms sitting at the surface, the subsurface, and the innermost layer for majority- and minority-spin components in the LDA (left panel) and in the DMFT approach (right panel).
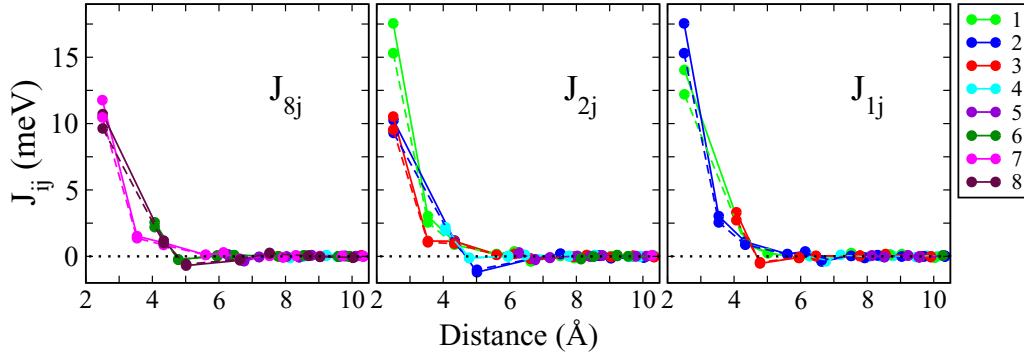
FIG. 8. (Color online) Layer-resolved exchange parameters (J_{ij}) for a 15-layer hcp Co (0001) slab for the case when atom i is located in the innermost layer (left panel), in the subsurface (middle panel), and at the surface (right panel). The solid lines indicate LDA results while the dashed lines represent the LDA+DMFT results. The layer numbering in the legend starts from the surface denoted by 1, the subsurface denoted by 2, and so on. The innermost layer is denoted by 8. The interaction between the surface and layer 9 and others is small and is not shown in these plots.

mostly arises from $d_{x^2-y^2}$ and d_{xy} contributions, is slightly suppressed and shifted to lower energies for atoms at the surface. Conversely, at the surface, there is a slight increase in the spectral weight around the Fermi level for the minority-spin states. This weight is mainly due to orbitals with d_{yz} and d_{xz} symmetry. In addition, as we saw for the case of Fe, this will result in larger values for the local exchange field (Σ^s) at the surface, and consequently in larger exchange integrals. Finally, Fig. 7 also shows that the PDOSs obtained from LDA and LDA+DMFT show similar features around the Fermi level. Hence, one would expect a similar trend in the asymptotic behavior of the exchange parameters obtained within these two methods.

In Fig. 8, layer-resolved exchange parameters are displayed for the physically most interesting layers. Results from both LDA and LDA+DMFT are reported. In contrast to the Fe slab, a relatively faster decay of the exchange parameters can be seen for the Co slab. This is due to the fact that the Ruderman-Kittel-Kasuya-Yosida (RKKY) character is less effective in strong magnets, e.g., as pointed out in Ref. [52]. However, itinerant magnets, in general, are not perfect strong magnets, due to the hybridization between d orbitals and sp states. Our statement of strong ferromagnetism in this paper should be viewed as describing a situation when the majority-spin states of the DOS are completely filled and hence pushed below the Fermi level.

In agreement with the results for the Fe slab, we obtained that the *interlayer* exchange parameters between NNs are substantially smaller in the inner layers than in layers close to the surface (for comparison, see the green lines in the middle panel of Fig. 8 and the pink lines in the left panel). However, in contrast to the Fe surface, there is a strong *intralayer* FM coupling between the NN at the Co surface, both in LDA and in LDA+DMFT (light green lines in the right panel). An analysis of individual orbital contributions to these exchange parameters reveals the there are strong FM contributions arising from all $3d$ orbitals where the $d_{yz}-d_{yz}$ and $d_{xy}-d_{xy}$ contributions are the strongest.

Despite the strong intralayer and interlayer FM coupling between atoms at the surface, the associated total exchange interaction (J_1) is still smaller than those obtained for the inner

layers, due to the lower coordination number. As for Fe, the consequence is in qualitative agreement with the conclusions reported by Turek *et al.* [32], but the magnitude is very dependent on the number of shells included in the calculation of J_1.

As seen in Fig. 8, both LDA and LDA+DMFT approaches deliver quite similar results for the exchange parameters. The only difference, as we saw for the case of Fe, is the reduction in magnitude of the J_{ij}'s obtained within the LDA+DMFT approach, while the overall behavior is similar and the sign is the same.

C. Ni

Finally, we have considered a slab of fcc Ni consisting of 15 layers repeated in the (001) direction. In Fig. 9, the PDOSs for atoms in the innermost (middle), subsurface, and surface layers are reported, for both LDA and LDA+DMFT. The PDOS for an atom in the innermost layer is similar to that of an atom at the subsurface, especially in the vicinity of E_F. Discrepancies are visible at higher binding energies, where the peaks become narrower at the subsurface. These differences are small. Around the Fermi level, the PDOS of the majority spin for atoms at the surface is similar to that for the innermost layer.
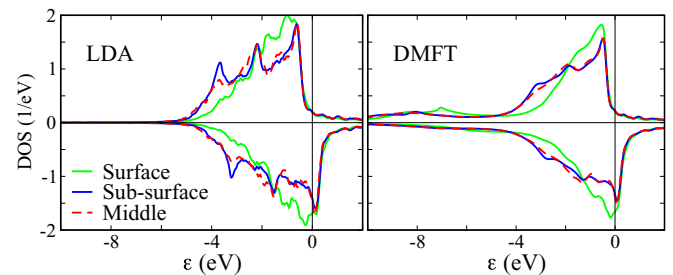
FIG. 9. (Color online) Layer-resolved projected density of states of $3d$ orbitals of a Ni slab for the atoms sitting at the surface, the subsurface, and the innermost layer for majority- and minority-spin components in the LDA (left panel) and in the DMFT approach (right panel).
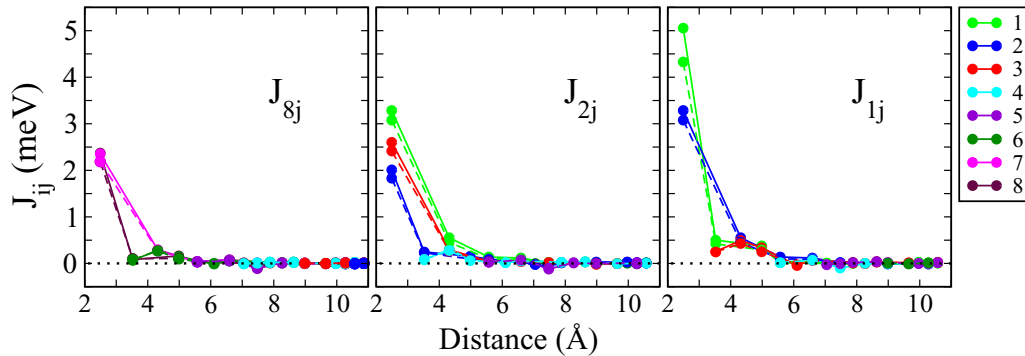
FIG. 10. (Color online) Layer-resolved exchange parameters (J_{ij}) for a 15-layer fcc Ni(001) slab for the case when atom i is located in the innermost layer (left panel), in the subsurface (middle panel), and at the surface (right panel). The solid lines indicate LDA results while the dashed lines represent the LDA+DMFT results. The layer numbering in the legend starts from the surface denoted by 1, the subsurface denoted by 2, and so on. The innermost layer is denoted by 8. The interaction between the surface and layer 9 and others is small and is not shown in these plots.

Minority-spin states, instead, show some differences between atoms at the surface and in the innermost layer. These differences originate mainly from the fact that the surface exhibits a larger contribution of d_{z^2} and $d_{x^2-y^2}$ states to the E_F.

Similarly to Fe and Co, the PDOSs obtained via LDA and LDA+DMFT are rather similar around the Fermi level, but they possess stronger differences at higher excitations energies.

Layer-resolved exchange parameters for Ni are reported in the top panel of Fig. 10 for both LDA and LDA+DMFT. Similar to the case of hcp Co, a relatively fast decay in exchange parameters with distance has been observed. This is consistent with the less pronounced RKKY character reported for bulk strong ferromagnets [52]. However, the magnitude of the coupling for Ni is shown to be about three times smaller than that for Co. As in the case of Fe and Co, the NN interlayer exchange parameters are larger for the layers close to the surface (for comparison, see the pink lines in the left panel and the green lines in the middle panel). As we have seen for the Co surface, there is a FM in-plane exchange coupling between the NN at the surface of Ni both in the LDA and LDA+DMFT approaches (green lines in the right panel).

Interestingly, the sum of all of the exchange parameters for atoms at the surface (J_1) is significantly larger than the corresponding sum (J_2) at the subsurface for both LDA and LDA+DMFT. This amount is 47.96 (41.87) meV in LDA (LDA+DMFT) for the surface versus 46.36 (41.35) meV for the subsurface. This might seem to be in contrast to the fact that a lower coordination number should lead to a lower total exchange parameter. However, Eq. (2) shows that the dependence on the exchange splitting is more relevant, which explains our results for Fe, Co, and Ni. We should also mention that here all of the exchange parameters are evaluated inside a shell of 10 Å radius.

D. Spin and orbital moments

As mentioned above, all calculations presented so far were performed in the scalar relativistic limit. It is interesting to analyze the influence of spin-orbit coupling on the magnetic

properties of Fe, Co, and Ni surfaces. Therefore, we have performed additional relativistic calculations including spin-orbit coupling corrections, whose results are reported in Table II. Our results for the innermost layers are in qualitative agreement with a prior study for bulk [28] and for the surface [17,58,59]. Comparing the results of the Fe slab in Table II between the LDA and LDA+DMFT approaches reveals that in general DMFT tends to improve the results of the LDA for the slabs both in the bulklike and in the surface regions. This improvement is not only on the magnitude of spin and orbital moments but also in their ratio (μ_l/μ_s), which for bcc Fe is about 0.023 (0.028) for the LDA (DMFT), as can be deduced from Table II. The experimental value reported for bcc Fe bulk is about 0.037 [53]. For the surface spins, the enhancement of μ_l/μ_s is even larger (0.033 in LDA and 0.046 in DMFT) thanks to the more pronounced orbital polarizations at the surface rising from more localized states. For hcp Co and fcc Ni, similar conclusions can be drawn. DMFT enhances the value of the orbital moment, both for bulk and surface atoms. For fcc Ni, the experimental values of the bulk are in good agreement with theory, while for Fe and Co the theory underestimates the value of the bulk orbital moment by 15–25%. However, DMFT provides a systematically better approach to investigate the orbital moments of these materials, at least judging from the bulk values. Unfortunately, surface orbital moments are not frequently reported for these materials, and we list in Table II one measured value of fcc Co (on a Cu 001 substrate) that shows enhancement compared to bulk values. On the other hand, spin moments obtained from the LDA are marginally modified by the dynamical correlations.

Finally, we should mention that our results for (μ_l/μ_s) are not quantitatively comparable to some of the recent experimental data based on electron magnetic circular dichroism (EMCD), which have reported higher values for this ratio (0.08 ± 0.01 for bcc Fe in Ref. [60] and 0.14 ± 0.03 for hcp Co in Ref. [61]). However, we found a closer agreement between the theoretical results and the experimental data based on x-ray magnetic circular dichroism (XMCD), as shown in Table II [53–55].

TABLE II. Layer-resolved spin (μ_s) and orbital moment (μ_o) for Fe, Co, and Ni slabs using the LDA (DMFT) approach including spin-orbit coupling corrections as well as the experimental values.

	Fe		Co		Ni	
	μ_s^{calc}	μ_l^{calc}	μ_s^{calc}	μ_l^{calc}	μ_s^{calc}	μ_l^{calc}
Surface	2.92 (2.94)	0.107 (0.122)	1.75 (1.79)	0.086 (0.122)	0.75 (0.77)	0.066 (0.080)
Subsurface	2.32 (2.36)	0.057 (0.067)	1.68 (1.73)	0.077 (0.111)	0.67 (0.68)	0.055 (0.067)
Middle	2.20 (2.24)	0.051 (0.063)	1.65 (1.70)	0.076 (0.108)	0.63 (0.65)	0.047 (0.057)
	μ_s^{calc}	μ_l^{calc}	μ_s^{calc}	μ_l^{calc}	μ_s^{calc}	μ_l^{calc}
Bulk	2.15[a]	0.080[a]	1.52[a]	0.140[a]	0.51[a]	0.043[a]
Bulk	2.08[b]	0.092[b]	1.52[b]	0.147[b]	0.52[b]	0.051[b]
Bulk	1.98[c]	0.085[c]	1.62[c]	0.154[c]	0.65[d]	0.055[d]
Bulk			1.86[e]	0.130[e]		
Bulk			1.72[f]	0.134[f]		
Surface			1.92[f]	0.234[f]		

[a]Reference [53].
[b]Reference [54].
[c]Reference [55].
[d]Reference [56].
[e]Reference [57].
[f]Reference [19]. These values are for fcc Co.

IV. CONCLUSIONS

In this work, we have investigated the interatomic exchange of bcc Fe, hcp Co, and fcc Ni as one comes closer to the surfaces from the bulk region. Our theoretical method is based both on the local spin-density approximation and dynamical mean-field theory, in which dynamic correlations are treated explicitly. We have used a slab geometry in these studies, and we found that for the central layers of the slabs, bulklike moments and exchange parameters are found in all three studied cases. As one approaches the surface region from the bulk, will observe a general trend of enhanced spin and orbital moments, both in LSDA and in DMFT. In fact, the difference between the results of LSDA and DMFT is rather minor for these systems, at least when it comes to spin moments and interatomic exchange parameters. For the orbital moments, we observe somewhat larger differences between LSDA and DMFT results, and we find that the latter generally compare better to experiments, where a comparison is possible.

A more detailed inspection of the interatomic exchange interactions reveals a general trend of enhanced values at the surfaces. We find that this is primarily driven by the increased exchange splitting of the surface states, something that is caused by the reduced coordination number of surface atoms. Hence, the experimental observation of lower ordering temperatures of surfaces, which is a general phenomenon, is not caused by a reduction of the interatomic exchange interactions of the surfaces. In contrast, the surface exchange interactions are enhanced. However, when coupled to an effective spin-Hamiltonian, of Heisenberg type or similar, the reduced coordination of surface atoms reduced the local Weiss field of the surface atoms, which makes them more susceptible to thermal fluctuations.

Finally, we have analyzed symmetry-resolved aspects of nearest-neighbor interactions of surface atoms of bcc Fe, and we found that some of these interactions are ferromagnetic whereas some are antiferromagnetic, and that summed over all symmetry components, the nearest-neighbor exchange interaction of surface atoms is antiferromagnetic. The magnetic order of the Fe surface is nevertheless ferromagnetic, due to strong ferromagnetic coupling to subsurface atoms. We argue, however, that the antiferromagnetic surface interactions of bcc Fe are inherent, and they should be an avenue to tune complex magnetic structures of monatomic overlayers of Fe on bcc substrates.

APPENDIX A: THE EFFECT OF U ON J_{ij}

At the surface, because of the less effective screening, the value of the Hubbard U is expected to increase. In this regard, we performed a series of calculations using higher values for the surface and subsurface atoms to see the impact of U on the exchange parameters. For Fe, we have used $U = 3$ eV for atoms at the surface and $U = 2.8$ eV for those on the subsurface, while the value for the inner layers is kept fixed to 2.3 eV. The outcome of these calculations, together with the results obtained with a uniform U value (2.3 eV) for all atoms, are shown in Fig. 11. It is evident that larger U values for surface atoms result in a small uniform reduction of the parameters J_{ij}, but the trends are unchanged (compare the
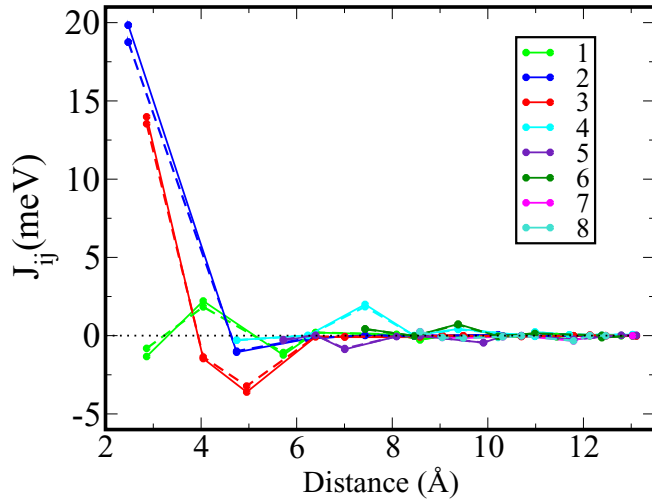
FIG. 11. (Color online) Layer-resolved exchange parameters (J_{ij}) for the surface atom of bcc Fe (atom i is located at layer 1). The solid lines indicate the results obtained for $U = 2.3$ eV for all atoms, and the dashed lines represent the results for layer-dependent U values (see the text). The layer numbering starts from the surface denoted by 1, the subsurface is denoted by 2, and so on.

dashed lines with the solid lines in Fig. 11). From the extent of these changes we conclude that the overall behavior, in particular the sign of the coupling, does not change if U is varied within a reasonable range. Finally, similar conclusions can be obtained from analogous calculations for Co and Ni, which confirms that the values of the exchange parameters are rather robust with respect to the choice of the U value.

APPENDIX B: CHARGE SELF-CONSISTENCY

The results presented in the main text refer to calculations in which the electron density is kept fixed to its LDA value, and the local correlation effects affect the results only through
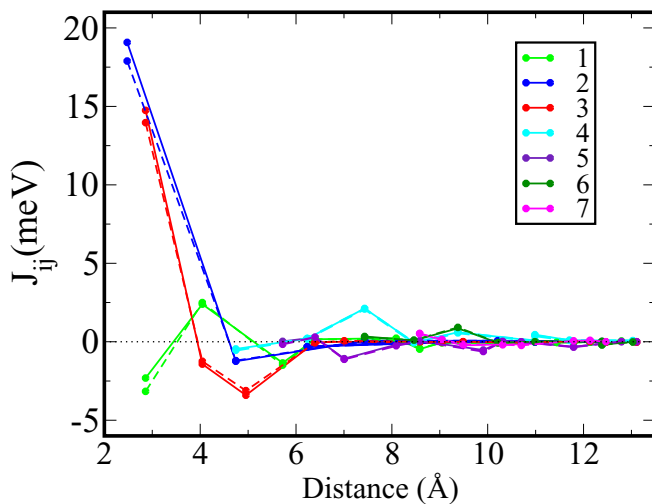
FIG. 12. (Color online) Layer-resolved exchange parameters (J_{ij}) for the surface atom of a seven-layer Fe slab (atom i is located at layer 1). The solid (dashed) lines indicate the results without (with) updating the electron density. The layer numbering starts from the surface denoted by 1, the subsurface denoted by 2, and so on.

the self-energy function. However, we performed several calculations to analyze the role of complete self-consistency over the electron density. We illustrate these results for a seven-layer slab of Fe(001). The obtained exchange parameters for one atom at the surface are reported in Fig. 12, with and without updating the electron density. One can observe only small variations in the absolute magnitude of the parameters J_{ij}. These differences amount to only a few percent. Similar calculations have been performed for seven-layer slabs of Co and Ni, and they lead to similar results. Thus, we conclude that the effects of charge self-consistency within the LDA+DMFT scheme are negligible for treating the magnetic properties of the transition-metal surfaces. This may be important for future investigations of thin films deposited on a substrate, where computational efficiency is going to be of primary importance.

APPENDIX C: STRENGTH OF MANY BODY EFFECTS

In this Appendix, we show the results for the calculated orbital-resolved renormalization factors Z in slabs of Fe, Co, and Ni. Z_m^σ denotes the inverse of an effective-mass enhancement for the correlated orbital m, and it is defined as

$$Z_m^\sigma = \left(1 - \frac{d \operatorname{Re}\Sigma_{mm}^\sigma(\omega)}{d\omega}\bigg|_{\omega=0}\right)^{-1}, \qquad (\text{C1})$$

where $\Sigma_{mm}^\sigma(\omega)$ is the self-energy projected on the orbital m with the spin projection σ, and $\omega = 0$ corresponds to E_F. In general, Z-factors are good measures of the strength of the correlation effects. To have a compact description of the latter, we have also calculated the average Z_{av}^σ per spin channel. Z_{av}^σ was computed using the following expression:

$$Z_{av}^\sigma = \frac{\sum_m Z_m^\sigma N_m(E_F)}{\sum_m N_m(E_F)}, \quad m = d_{z^2}, \dots, d_{xy}, \qquad (\text{C2})$$

where $N_m^\sigma(E_F)$ denotes the partial density of states at the Fermi level of a particular state. Thus, the average Z-factor is a weighted sum of orbital-resolved renormalization factors. The weight of each orbital is defined by its relative contribution to the spectral weight at the Fermi level.

Calculated values of orbital-resolved Z-factors as well as their average values are shown in Table III. An inspection of the results suggests that overall the correlation effects in all studied systems are not very strong (as a limiting case, $Z = 1$ corresponds to the LDA). In Co and Ni slabs, the renormalization factors for all $3d$ orbitals are similar and their values lie in the range between 0.7 and 0.8. It is also seen that the many-body effects are the most pronounced for surface electrons. The largest renormalization effects are found for the Fe slab. In particular, majority-spin electrons of the surface atoms experience a mass enhancement that is almost twice as large. Their overall spectral weight at E_F is relatively small (see Fig. 3), and thus these quasiparticles are more sensitive to the addition of the self-energy.

Here we emphasize again the fact that the differences in the Z-factors for majority and minority electrons are quite substantial. However, within a particular spin channel the orbital-resolved Z-factors show relatively smaller deviations from the average value.

TABLE III. Orbital-resolved and average (av) renormalization factors Z for Fe, Co, and Ni slabs.

	Fe											
	Majority spin						Minority spin					
	d_{z^2}	$d_{x^2-y^2}$	d_{yz}	d_{xz}	d_{xy}	av	d_{z^2}	$d_{x^2-y^2}$	d_{yz}	d_{xz}	d_{xy}	av
Surface	0.57	0.54	0.51	0.51	0.54	0.53	0.76	0.72	0.74	0.74	0.72	0.73
Subsurface	0.73	0.72	0.72	0.72	0.72	0.72	0.78	0.77	0.81	0.81	0.81	0.80
Middle	0.72	0.72	0.71	0.71	0.71	0.71	0.76	0.76	0.76	0.76	0.76	0.76
	Co											
	Majority spin						Minority spin					
	d_{z^2}	$d_{x^2-y^2}$	d_{yz}	d_{xz}	d_{xy}	av	d_{z^2}	$d_{x^2-y^2}$	d_{yz}	d_{xz}	d_{xy}	av
Surface	0.73	0.75	0.74	0.74	0.75	0.74	0.73	0.78	0.75	0.75	0.78	0.76
Subsurface	0.78	0.77	0.77	0.77	0.77	0.77	0.82	0.81	0.82	0.82	0.81	0.81
Middle	0.78	0.77	0.76	0.76	0.77	0.77	0.82	0.81	0.81	0.81	0.81	0.81
	Ni											
	Majority spin						Minority spin					
	d_{z^2}	$d_{x^2-y^2}$	d_{yz}	d_{xz}	d_{xy}	av	d_{z^2}	$d_{x^2-y^2}$	d_{yz}	d_{xz}	d_{xy}	av
Surface	0.78	0.77	0.79	0.79	0.78	0.78	0.69	0.69	0.68	0.68	0.71	0.69
Subsurface	0.82	0.82	0.80	0.80	0.81	0.81	0.77	0.75	0.75	0.75	0.75	0.75
Middle	0.81	0.81	0.80	0.80	0.80	0.81	0.76	0.76	0.74	0.74	0.74	0.75

[1] K. von Bergmann, M. Bode, A. Kubetzka, O. Pietzsch, E. Vedmedenko, and R. Wiesendanger, Philos. Mag. **88**, 2627 (2008).

[2] F. Yildiz, M. Przybylski, and J. Kirschner, Phys. Rev. Lett. **103**, 147203 (2009).

[3] A. Bergman, L. Nordstöm, A. B. Klautau, S. Frota-Pessôa, and O. Eriksson, J. Magn. Magn. Mater. **320**, 1173 (2008).

[4] T. Ślęzak, M. Ślęzak, M. Zając, K. Freindl, A. Kozioł-Rachwał, K. Matlak, N. Spiridis, D. Wilgocka-Ślęzak, E. Partyka-Jankowska, M. Rennhofer, A. I. Chumakov, S. Stankov, R. Rüffer, and J. Korecki, Phys. Rev. Lett. **105**, 027206 (2010).

[5] A. Kubetzka, P. Ferriani, M. Bode, S. Heinze, G. Bihlmayer, K. von Bergmann, O. Pietzsch, S. Blügel, and R. Wiesendanger, Phys. Rev. Lett. **94**, 087204 (2005).

[6] M. Takada, P. Gastelois, M. Przybylski, and J. Kirschner, J. Magn. Magn. Mater. **329**, 95 (2013).

[7] P. Ferriani, S. Heinze, G. Bihlmayer, and S. Blügel, Phys. Rev. B **72**, 024452 (2005).

[8] R. B. Muniz, A. T. Costa, and D. L. Mills, J. Phys.: Condens. Matter **15**, S495 (2003).

[9] A. Al-Zubi, G. Bihlmayer, and S. Blügel, Phys. Rev. B **83**, 024407 (2011).

[10] J. Kudrnovský, F. Máca, I. Turek, and J. Redinger, Phys. Rev. B **80**, 064405 (2009).

[11] L. Liebermann, J. Clinton, D. M. Edwards, and J. Mathon, Phys. Rev. Lett. **25**, 232 (1970).

[12] J. Kortright, D. Awschalom, J. Stöhr, S. Bader, Y. Idzerda, S. Parkin, I. K. Schuller, and H.-C. Siegmann, J. Magn. Magn. Mater. **207**, 7 (1999).

[13] D.-s. Wang, A. J. Freeman, and H. Krakauer, Phys. Rev. B **26**, 1340 (1982).

[14] O. Jepsen, J. Madsen, and O. K. Andersen, Phys. Rev. B **26**, 2790 (1982).

[15] E. Wimmer, A. J. Freeman, and H. Krakauer, Phys. Rev. B **30**, 3113 (1984).

[16] P. Bruno, Phys. Rev. B **39**, 865 (1989).

[17] O. Eriksson, A. M. Boring, R. C. Albers, G. W. Fernando, and B. R. Cooper, Phys. Rev. B **45**, 2868 (1992).

[18] O. Eriksson, G. Fernando, R. Albers, and A. Boring, Solid State Commun. **78**, 801 (1991).

[19] M. Tischer, O. Hjortstam, D. Arvanitis, J. H. Dunn, F. May, K. Baberschke, J. Trygg, J. M. Wills, B. Johansson, and O. Eriksson, Phys. Rev. Lett. **75**, 1602 (1995).

[20] P. Hohenberg and W. Kohn, Phys. Rev. **136**, B864 (1964).

[21] E. Runge and E. K. U. Gross, Phys. Rev. Lett. **52**, 997 (1984).

[22] N. D. Mermin, Phys. Rev. **137**, A1441 (1965).

[23] D. Chandesris, J. Lecante, and Y. Petroff, Phys. Rev. B **27**, 2630 (1983).

[24] C. Guillot, Y. Ballu, J. Paigné, J. Lecante, K. P. Jain, P. Thiry, R. Pinchaux, Y. Pétroff, and L. M. Falicov, Phys. Rev. Lett. **39**, 1632 (1977).

[25] A. I. Lichtenstein, M. I. Katsnelson, and G. Kotliar, Phys. Rev. Lett. **87**, 067205 (2001).

[26] J. Braun, J. Minár, H. Ebert, M. I. Katsnelson, and A. I. Lichtenstein, Phys. Rev. Lett. **97**, 227601 (2006).

[27] A. Grechnev, I. Di Marco, M. I. Katsnelson, A. I. Lichtenstein, J. Wills, and O. Eriksson, Phys. Rev. B **76**, 035107 (2007).

[28] S. Chadov, J. Minár, M. I. Katsnelson, H. Ebert, D. Ködderitzsch, and A. I. Lichtenstein, Europhys. Lett. **82**, 37001 (2008).

[29] A. I. Lichtenstein and M. I. Katsnelson, Phys. Rev. B **57**, 6884 (1998).

[30] G. Kotliar, S. Y. Savrasov, K. Haule, V. S. Oudovenko, O. Parcollet, and C. A. Marianetti, Rev. Mod. Phys. **78**, 865 (2006).

[31] V. I. Anisimov, A. I. Poteryaev, M. A. Korotin, A. O. Anokhin, and G. Kotliar, J. Phys.: Condens. Matter **9**, 7359 (1997).

[32] I. Turek, J. Kudrnovsky, V. Drchal, and P. Bruno, Philos. Mag. **86**, 1713 (2006).

[33] T.-H. Chuang, K. Zakeri, A. Ernst, Y. Zhang, H. J. Qin, Y. Meng, Y.-J. Chen, and J. Kirschner, Phys. Rev. B **89**, 174404 (2014).

[34] Y. Meng, K. Zakeri, A. Ernst, T.-H. Chuang, H. J. Qin, Y.-J. Chen, and J. Kirschner, Phys. Rev. B **90**, 174437 (2014).

[35] A. Deák, L. Szunyogh, and B. Ujfalussy, Phys. Rev. B **84**, 224413 (2011).

[36] A. I. Liechtenstein, M. I. Katsnelson, V. P. Antropov, and V. A. Gubanov, J. Magn. Magn. Mater. **67**, 65 (1987).

[37] J. M. Wills, M. Alouani, P. Andersson, A. Delin, O. Eriksson, and O. Grechnyev, in *Full-Potential Electronic Structure Method*, edited by E. S. H. Dreysse, Springer Series in Solid-State Sciences (Springer-Verlag, Berlin, 2010).

[38] P. Thunström, I. Di Marco, A. Grechnev, S. Lebègue, M. I. Katsnelson, A. Svane, and O. Eriksson, Phys. Rev. B **79**, 165104 (2009).

[39] O. Grånäs, I. Di Marco, P. Thunström, L. Nordström, O. Eriksson, T. Björkman, and J. M. Wills, Comput. Mater. Sci. **55**, 295 (2012).

[40] M. I. Katsnelson and A. I. Lichtenstein, Phys. Rev. B **61**, 8906 (2000).

[41] Y. O. Kvashnin, O. Grånäs, I. Di Marco, M. I. Katsnelson, A. I. Lichtenstein, and O. Eriksson, Phys. Rev. B **91**, 125133 (2015).

[42] H. Li, Y. S. Li, J. Quinn, D. Tian, J. Sokolov, F. Jona, and P. M. Marcus, Phys. Rev. B **42**, 9195 (1990).

[43] M. P. Marder, *Condensed Matter Physics* (Wiley, Hoboken, NJ, 2010).

[44] M. I. Katsnelson and A. I. Lichtenstein, Eur. Phys. J. B **30**, 9 (2002).

[45] V. I. Anisimov, F. Aryasetiawan, and A. I. Lichtenstein, J. Phys.: Condens. Matter **9**, 767 (1997).

[46] W. A. Harrison, *Solid State Theory* (McGraw-Hill, New York, 1970).

[47] D. Vieira, H. J. Freire, V. C. Jr., and K. Capelle, J. Magn. Magn. Mater. **320**, e418 (2008), Latin American Workshop on Magnetism, Magnetic Materials and their Applications.

[48] R. Wu and A. J. Freeman, Phys. Rev. B **45**, 7532 (1992).

[49] S. Polesya, O. Šipr, S. Bornemann, J. Minár, and H. Ebert, Europhys. Lett. **74**, 1074 (2006).

[50] J. Schäfer, M. Hoinkis, E. Rotenberg, P. Blaha, and R. Claessen, Phys. Rev. B **72**, 155115 (2005).

[51] V. V. Mazurenko, S. N. Iskakov, A. N. Rudenko, I. V. Kashin, O. M. Sotnikov, M. V. Valentyuk, and A. I. Lichtenstein, Phys. Rev. B **88**, 085112 (2013).

[52] M. Pajda, J. Kudrnovský, I. Turek, V. Drchal, and P. Bruno, Phys. Rev. B **64**, 174402 (2001).

[53] M. B. Stearns, *Magnetic Properties of 3d, 4d and 5d Elements and Their Alloys and Compounds*, Landolt-Börnstein (Springer, Berlin, 1984).

[54] R. A. Reck and D. L. Fry, Phys. Rev. **184**, 492 (1969).

[55] C. T. Chen, Y. U. Idzerda, H.-J. Lin, N. V. Smith, G. Meigs, E. Chaban, G. H. Ho, E. Pellegrin, and F. Sette, Phys. Rev. Lett. **75**, 152 (1995).

[56] H. A. Mook, Phys. Rev. **148**, 495 (1966).

[57] R. M. Moon, Phys. Rev. **136**, A195 (1964).

[58] M. Aldén, H. Skriver, S. Mirbt, and B. Johansson, Surf. Sci. **315**, 157 (1994).

[59] A. Huda and A. Mookerjee, J. Magn. Magn. Mater. **267**, 97 (2003).

[60] H. Lidbaum, J. Rusz, A. Liebig, B. Hjörvarsson, P. M. Oppeneer, E. Coronel, O. Eriksson, and K. Leifer, Phys. Rev. Lett. **102**, 037201 (2009).

[61] P. Schattschneider, S. Rubino, M. Stoeger-Pollach, C. Hebert, J. Rusz, L. Calmels, and E. Snoeck, J. Appl. Phys. **103**, 07D931 (2008).